13th ewtec 2019 Proceedings of the 13th European Wave and Tidal Energy Conference 1-6 Sept 2019, Naples, Italy

Numerical study of an inclined OWC chamber combined breakwater and turbine interaction under waves

Jeong-Seok Kim, Bowoo Nam, Kyong-Hwan Kim, Sewan Park, Keyyong Hong

Abstract—**In this study, the effect of wave field changes due to breakwaters on the performance of oscillating-water-column (OWC) type wave energy converter (WEC). A time-domain numerical method based on a three-dimensional potential flow solver is applied to compute the wave field around an inclined OWC chamber combined with the breakwater. Boundary value problem of Laplace equation is directly solved by using a finite element method. The present numerical method is verified based on the comparison with previous research. From the numerical simulation results, the performance of the OWC device was affected by the change of the wave field around the chamber due to the scattered wave from the breakwater. The damping zone was introduced to describe the energy dissipation effect at the front of the breakwater, and the breakwater effects on the chamber are discussed based on the numerical simulation results.**

Keywords— **OWC, WEC, Breakwater, Finite element method, Potential flow.**

I. Introduction

RECENTLY, various types of wave energy converters (WECs) have been developed to extract electrical energy from the wave energy resource. The oscillating-water-column (OWC) type device is one of the most famous WECs. The device converts the wave motion into an oscillating airflow in the chamber and operates by rotating the generator with the air flow. The bottom fixed type chamber of this device is typically installed on the shoreline or coastal area [1]. The OWC-type WEC combined with the breakwater was introduced to reduce the construction cost of the chamber structure [2-3]. Also, there has been an effort to develop the inclined OWC chamber to reduce the size and improve the applicability to the rubble-mound breakwaters [4-8].

The OWC-type WEC combined with the breakwater is affected by the wave field changes due to the interaction between the device and the breakwater. This study focuses on this phenomenon by using a numerical method based on potential theory. Boundary value problem of the Laplace equation is solved by using a finite element method in time-domain.

II. Numerical Method

In this study, the influence of wave field changes due to breakwaters on an inclined OWC chamber was investigated by the boundary value problem. The three-dimensional numerical analysis is carried out in the time domain. Fig. 1 shows the schematic diagram of an inclined OWC chamber. The boundary value problem based on a linear potential theory can be formulated with respect to the Cartesian coordinate system. It is assumed that the fluid is inviscid and incompressible, and its flow is irrotational in the whole fluid domain.

Linearized boundary value problem is defined as:

$$\nabla^2\phi = 0 \qquad in\ \Omega \tag{1}$$

$$\frac{\partial\phi}{\partial t} = -g\zeta \qquad on\ S_F\ (\mathrm{z} = 0) \tag{2}$$

$$\frac{\partial\zeta}{\partial t} = \frac{\partial\phi}{\partial z} \qquad on\ S_F\ (\mathrm{z} = 0) \tag{3}$$

$$\frac{\partial\phi}{\partial n} = 0 \qquad on\ S_B \tag{4}$$

$$\frac{\partial\phi}{\partial n} = 0 \qquad on\ S_W \tag{5}$$

Governing equation for potential flow is the Laplace equation in Eq. (1). ϕ is velocity potential defined in the entire fluid domain Ω. Eqs. (2) and (3) show linearized

Paper ID number: 1285- Conference track: Wave hydrodynamic modelling.

This research was supported by a grant from National R&D Project "Development of Wave Energy Converters Applicable to Breakwater and Connected to Micro-Grid with Energy Storage System" funded by Ministry of Oceans and Fisheries, Korea (PMS3780).

All authors are with the Korea Research Institute of Ships and Ocean engineering (KRISO) 32, 1312, Daejeon, 34103 Korea

E-mail address for each author is as follows.

J.S. KIM (js-kim@kriso.re.kr).

B.W. Nam (bwnam@kriso.re.kr).

K.H. Kim (kkim@kriso.re.kr).

S.W. Park (sewanpark@kriso.re.kr).

K. Hong (khong@kriso.re.kr).

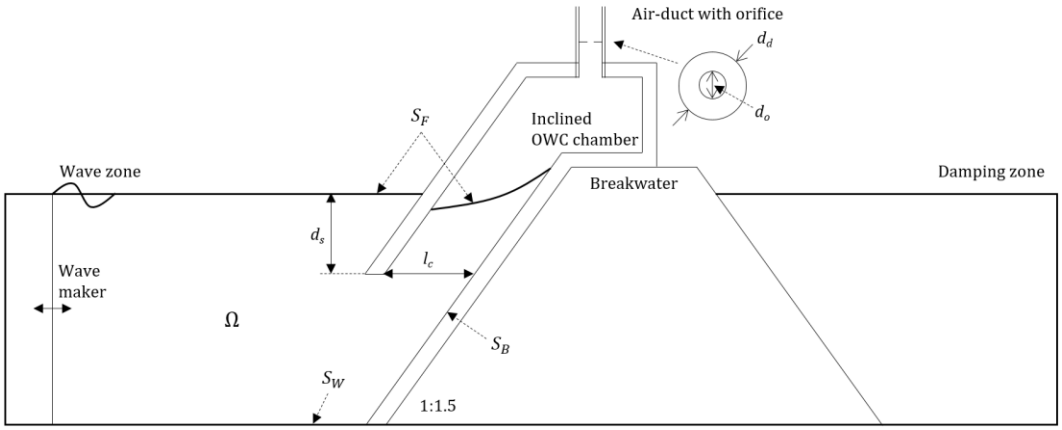

Fig. 1. Schematic diagram of an inclined OWC chamber with orifice model.

free-surface boundary conditions S_F. Here, $\zeta^{(1)}$ is the wave elevation on the free-surface. g is the gravitational acceleration constant. Eq. (4) is the body boundary condition for the inclined OWC chamber and breakwater. S_B is the wetted surface area of the body. Eq. (5) is the wall boundary condition S_W on the sea bottom. The superscripts indicate the order of the problem.

The weak formulation of the governing equation for the potential flow could be obtained by introducing the test function ψ and applying integration by parts in Eq. (6).

$$\iiint_{\Omega} \nabla\phi \cdot \nabla\Psi dV - \iint_{\partial\Omega} \frac{\partial\phi}{\partial n}\Psi dS = 0 \tag{6}$$

The fluid domain is discretized using a finite number of elements, and the velocity potential function is approximated as a linear summation of the continuous and differentiable test functions. The velocity potential and can be expressed as Eqs. (7) and (8) by applying Galerkin approximation.

$$\phi = \sum_i \phi_i N_i \tag{7}$$

$$\zeta = \sum_k \zeta_k M_k \tag{8}$$

where, N_i is a three-dimensional shape function for the entire fluid domain, and N_i is a two-dimensional shape function on the free surface. Eight-node hexahedral elements and four-node quadrilateral elements are used. The boundary value problem can be expressed as following a linear algebraic equations.

$$K_{ij}\phi_i^{(1)} = F_i \tag{9}$$

$$T_{ik}\dot{\zeta}_k^{(1)} = P_{ik}\left(\phi_{n,k}^{(1)} + f_{\zeta,k}\right) \tag{10}$$

$$T_{ik}\dot{\phi}_k^{(1)} = P_{ik}\left(-g\zeta_k^{(1)} + f_{\phi,k}\right) \tag{11}$$

$$K_{ij} = \iiint_{\Omega} \nabla N_i \cdot \nabla N_j dV \tag{12}$$

$$F_i = \iint_{S_B} \frac{\partial\phi}{\partial n} N_i dS \tag{13}$$

$$T_{ik} = P_{ik} = \iint_{S_F} M_i M_k dS \tag{14}$$

The solution of the Laplace equation is obtained from Eq. (7). The free-surface velocity potential and elevation are integrated in time by Eqs. (10) and (11). In the present study, the conjugate gradient method is employed for solving Eqs. (12) - (14). $f_{\zeta,k}$ and $f_{\phi,k}$ are forcing terms attributed to the velocity potential and wave elevation on the free surface, respectively.

The orifice model is introduced to simulate the pressure drop inside the chamber due to the operation of the turbine. The airflow passing through the orifice was calculated from the time variation of the air volume based on the integral of the surface elevation inside the chamber. The orifice model that can be represented as the relationship between the air-velocity (U) passing through the orifice and the pressure drop (ΔP) is as follows.

$$\Delta P = \mu U \tag{15}$$

An artificial damping zone is introduced to satisfy the pressure drop inside the. An artificial damping term is added to the velocity potential in the dynamic free-surface condition, and the wave elevation is forced to damp out in the kinematic free-surface condition. The artificial damping zone about two times of the wavelength is taken as the wave damping zone to satisfy the radiation condition numerically. The final free-surface

boundary conditions including the artificial damping terms are expressed as follows:

$$\frac{\partial \phi_D}{\partial t} = -g\zeta_D - \mu\phi_D \qquad on\ \mathrm{z} = 0 \qquad (16)$$

$$\frac{\partial \zeta_D}{\partial t} = \frac{\partial \phi_D}{\partial z} - \mu\zeta_D \qquad on\ \mathrm{z} = 0 \qquad (17)$$

where the subscript 'D' indicates the diffraction potential and waves. μ is the artificial damping coefficient for the strength of pressure drop acting on the free-surface inside the chamber.

III. VALIDATION OF NUMERICAL MODEL

The validity of the numerical model for the inclined OWC chamber with the orifice model is examined. Fig. 1 shows the schematic diagram for the inclined OWC chamber in a 2-D wave flume. This orifice model was set to simulate a pressure drop proportional to the air-velocity through the orifice in Eqs. (15) and (16).

For the verification of the present numerical model, the calculation results are directly compared with the existing CFD calculation results (Park et al., 2018). The CFD calculation results based on commercial software Star-CCM+ are presented in comparison with the model test results in a 2-D wave flume. In this case, the width (B_c) and length (l_c) of the OWC chamber are 10m and 5m. The draft of the skirt (d_s) is 2.0m. The slope of the structure is 1:1.5(=33.7°). The ratio of the orifice diameter (d_o) to the air-duct (d_d=0.8m) is d_o= 0.4d_d. Table I shows the wave condition for the verification of the numerical model. Fig. 2 shows the 2-D wave field around the inclined OWC chamber, which is calculated using the present numerical model. The waves are propagating from right to left. The OWC chamber is located on the left side.

TABLE I
WAVE CONDITIONS FOR VALIDATION TEST OF NUMERICAL MODEL

Wave Period T [s]	Wave Frequency ω [rad/s]	Wave Height H [m]	Wave Length λ [m]	Wave Steepness [-]
5.47	*1.15*	*0.40*	*42.25*	*0.009*
6.48	*0.97*	*0.46*	*53.93*	*0.009*
7.16	*0.88*	*0.48*	*61.60*	*0.008*
8.17	*0.77*	*0.48*	*72.80*	*0.007*
9.54	*0.66*	*0.39*	*87.48*	*0.004*

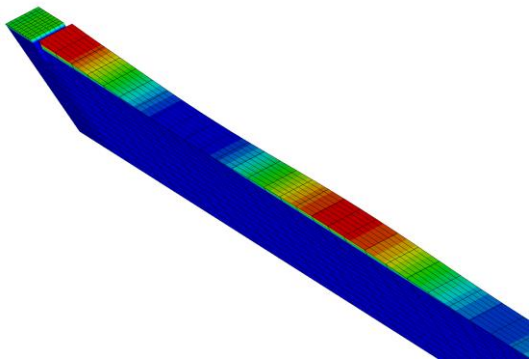

Fig. 2. Two-dimensional wave field around an inclined OWC chamber from numerical simulation.

Fig. 3 shows the comparison results of the OWC responses between the present model and the CFD results by Park et al. (2018). This figure shows (a) the relative wave height inside the chamber to incident wave height and normalized pneumatic responses for (b) the differential pressure and (c) the velocity of the airflow at the orifice. Here, H_I and A_I are the height and amplitude

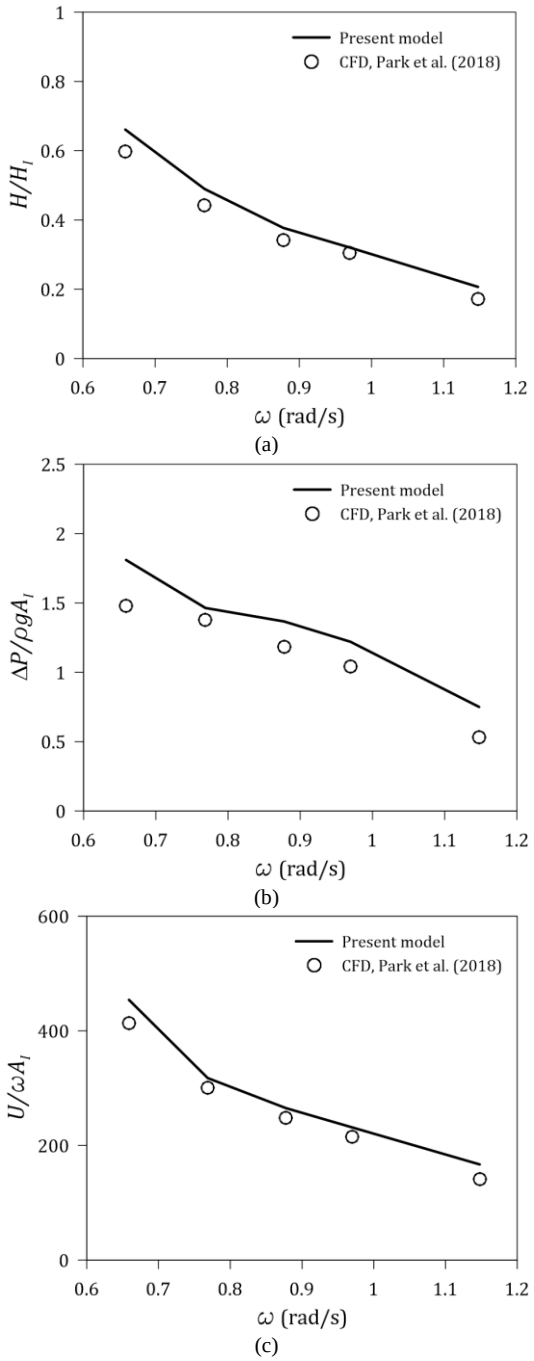

Fig. 3. Comparison of numerical analysis results between previous research and this study for an inclined OWC chamber with orifice model. (a) Relative wave height inside the chamber to incident wave height. Normalized pneumatic responses of (b) pressure drop and (c) air-velocity at the orifice.

of the incident wave. ρ is the density of water. ω is the angular frequency of the incident wave. Despite the differences in flow characteristics that can be considered in both models, the results are reasonably agreed for the small amplitude waves presented in Table I.

IV. BREAKWATER EFFECTS ON THE OWC CHAMBER

The effect of wave field changes due to scattered waves from breakwaters on OWC chamber performance was numerically investigated under the regular wave conditions. For efficient computation, half of the fluid domain in the transverse direction was applied to the simulation. Fig. 4 shows the computational grid around the OWC chamber and the breakwater. The numerical simulations were performed considering the interaction between the orifice and the chamber in the time domain.

The slope of the breakwater model is 1:1.5, which is the same as the OWC chamber. The length of the breakwater (L_{BW}) indicates the distance in the transverse direction from the side of the chamber. The breadth of the chamber is B_c. The surface of the chamber and breakwater correspond to the body boundary condition in Eq. (4). It was assumed that there was no energy dissipation effect on the surface and surrounding field of the breakwater.

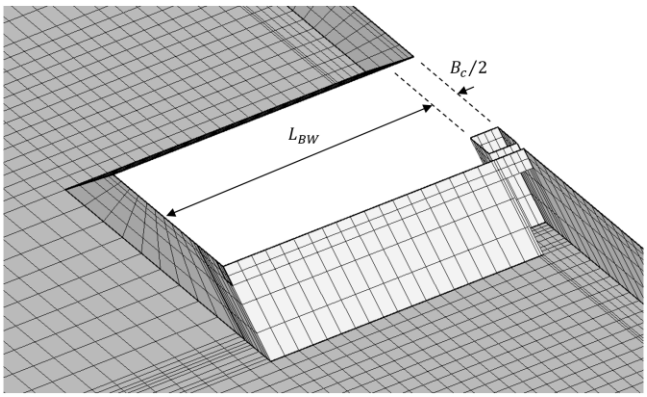

Fig. 4. Grid for an inclined OWC chamber with breakwater.

Fig. 5 shows the standing waves due to the combination of the incident and reflected wave in front of the breakwater. Fig. 5 (a) to (c), the incident wavelength ratios for the same breakwater length are 2.0, 1.0 and 0.75, respectively. It is shown that the spatial distribution of the standing waves formed in front of the breakwater is related to the ratio of the length between the incident wave and the breakwater. The standing wave was developed parallel to the breakwater in case of α corresponding to $\lambda/L_{BW} = 2.0$. On the other hand, when the wavelength is relatively shorter than the breakwater, it is shown that the spatial distribution of the standing waves formed in front of the breakwater is related to the ratio of the length between the incident wave and the breakwater. In order to analysis the correlation between the change of the surrounding wave field due to the breakwater and the performance of the OWC chamber, the length of the breakwater was set to be equal to the wavelength (λ_n) corresponding to the natural frequency

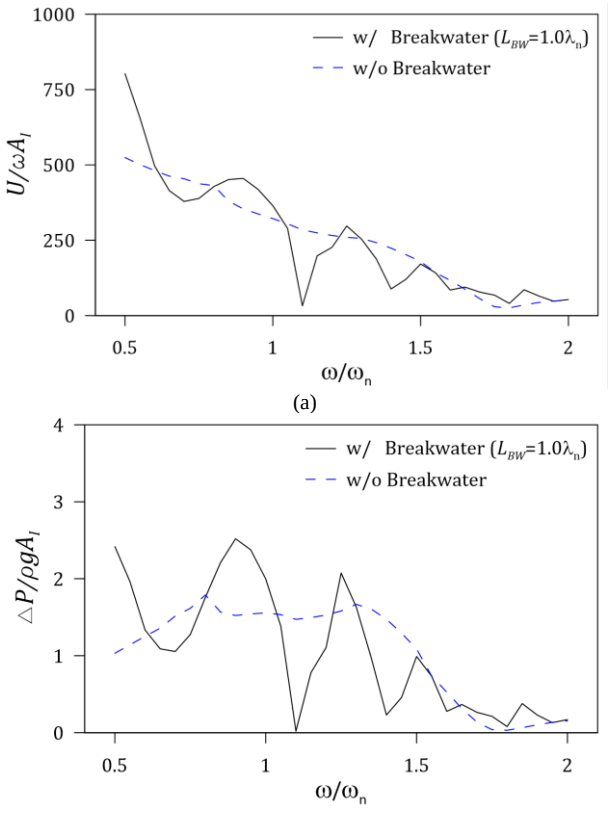

Fig. 6. Comparison of pneumatic responses of an inclined OWC chamber with (solid line) and without (dotted line) consideration of the breakwaters from numerical simulation results. Normalized values of (a) air-velocity and (b) pressure drop.

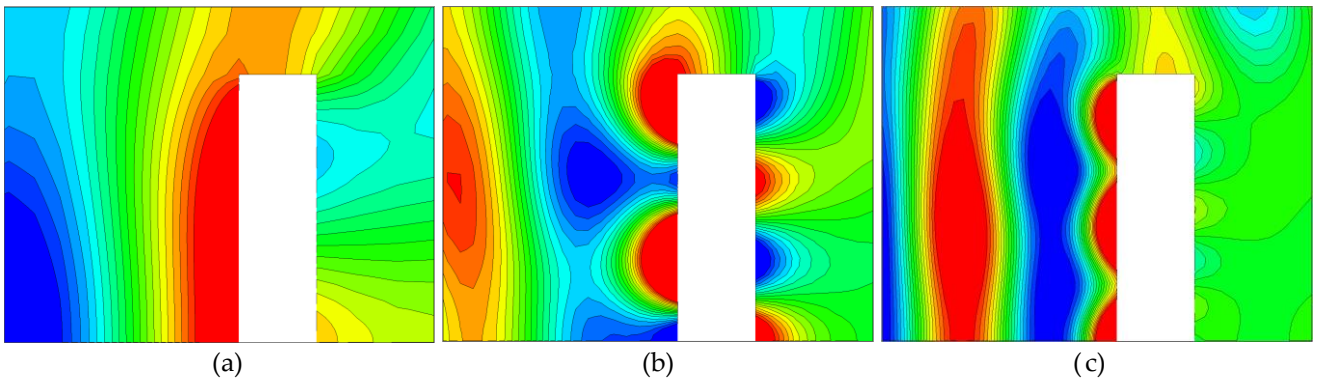

Fig. 5. Wave field around the breakwater from the numerical simulation.
(a) $\lambda/L_{BW} = 2.0$, (b) $\lambda/L_{BW} = 1.0$ and (c) $\lambda/L_{BW} = 0.75$.

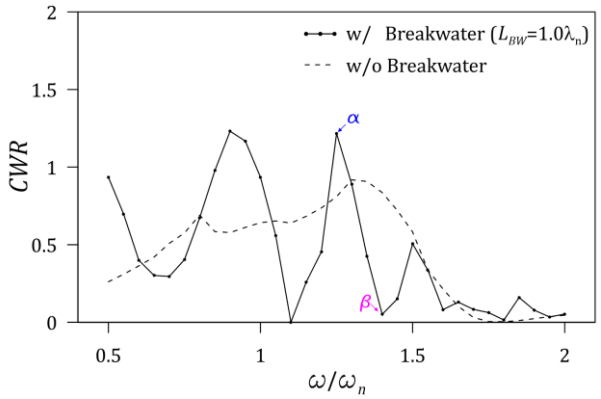

Fig. 7. Comparison of the capture width ratio of pneumatic power of an inclined OWC chamber with (solid line) and without (dotted line) consideration of the breakwaters from numerical simulation results.

($\omega_n = 0.85$ rad/s) of an inclined OWC chamber derived from the numerical simulation.

The normalized pneumatic responses according to the consideration of the breakwater model are compared in Fig. 6. In the OWC chamber-only simulation results (dotted line), the air-velocity (U) at the orifice showed critically-damped response and the differential pressure (ΔP) showed a large amplitude in the range of normalized frequency from 0.7 to 1.4 in Fig. 6(b). The pneumatic power (P) that can be calculated by multiplying ΔP and airflow rate ($Q = UA_o$) is shown in Fig. 7 as the capture width ratio (CWR). It is defined as the ratio of the absorbed wave power to the resource of the incident wave (J) [9]:

$$CWR = \frac{P}{JB_c} \tag{18}$$

The simulation results considering the breakwater model show that the pneumatic response increases or decreases with the wave frequency. Table II shows the wave conditions under which the change of pneumatic responses appeared. The difference in wave frequency between α and β, but the difference in the pneumatic responses was significant.

TABLE II
WAVE CONDITIONS FOR SPECIFIC CASES FOR THE BREAKWATER EFFECT

Case ID	ω [rad/s]	ω/ω_n	$\lambda/(L_{BW}+B_c/2)$
α	*1.0625*	*1.25*	*0.69*
β	*1.1900*	*1.40*	*0.58*

In order to analyze the effect of the breakwater affecting the performance of an inclined OWC chamber, the snapshots of the wave field for three combination cases depending on whether breakwater and chamber were considered are shown together in Fig. 8. All of the figures for α and β were captured at the peak of the pneumatic response in the numerical simulation result of case (c).

As shown in Fig. 7, no significant difference between α and β was observed in the surrounding wave field of chamber-only simulation results in Fig. 8(a). Regardless of the chamber considerations, the standing waves in front of the breakwater were similar in Figs. 8(b) and 8(c).

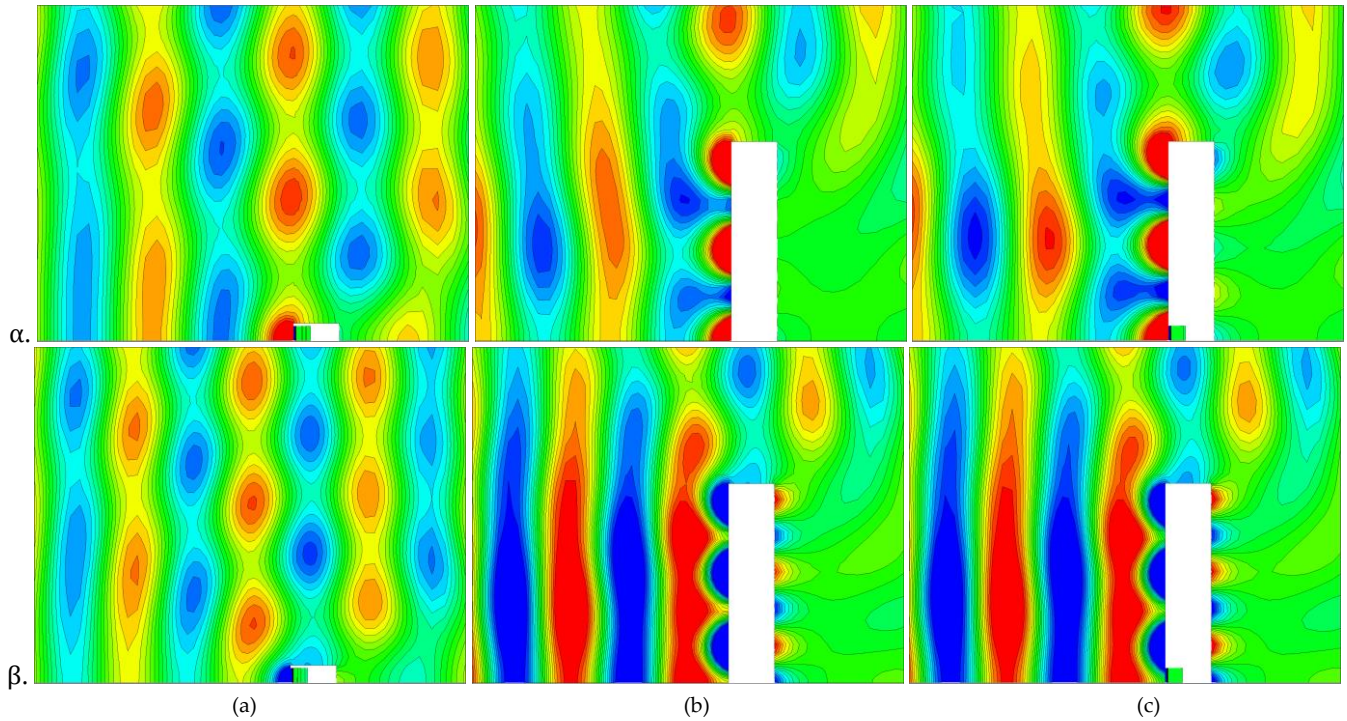

Fig. 8. Wave field around both breakwater and inclined OWC chamber from the numerical simulation for the wave conditions of α and β. The classification according to the model consideration (a) an inclined OWC chamber model, (b) a breakwater model and (c) an inclined OWC chamber with breakwater model.

These results imply that the dominant influence on the spatial distribution of the standing waves is the interaction between the breakwaters and incident waves. The variation of the *CWR* according to the wave frequency can be interpreted as the increase/decrease of the amount of wave energy into the OWC chamber depending on the node position of the standing wave developed due to the breakwaters.

However, the wave energy dissipates around the porous medium of the breakwater. Moreover, waves are scattered in many directions from the irregular surface of the breakwater and the armor layer. For this reason, the effect of the standing wave developed on the performance of the OWC chamber will be less than that shown in Fig. 7. In order to enhance the modeling of the breakwaters, a damping zone was introduced to simulate the dissipation of the wave energy due to armor layer such as tetrapod (TTP) installed in front of the breakwater in Fig. 9. The damping zone corresponds to Eqs. (15) and (16) with the artificial damping coefficient (μ).

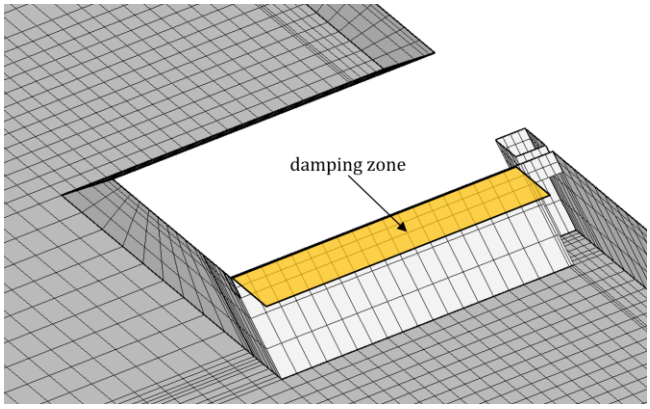

Fig. 9. Application of the damping zone to considering the wave energy dissipation due to tetrapod.

The surface elevation (η) in front of the breakwater according to the artificial damping coefficients is shown in Fig. 10 under the wave condition (α). The surface elevation was amplified up to 5 times as much as the incident wave, but gradually decreased with increasing damping coefficient. When the damping coefficient (μ) is 0.5, the free surface of the damping zone is forced to damp out, and the mode shape of the standing wave in the transverse direction is not shown well. It is shown that the introduction of the damping zone can describe the energy dissipation effect in front of the breakwater.

The variation of the *CWR* decreased with the dissipation of the wave energy at the front of the breakwater in Fig. 11. The pneumatic performance of the OWC chamber is changed according to the strength of the damping zone, which may imply that the modeling of the surrounding structure, as well as the chamber, is important in the performance assessment of OWC-type WECs. The reliability of the breakwater modeling can be improved by applying the artificial damping coefficient

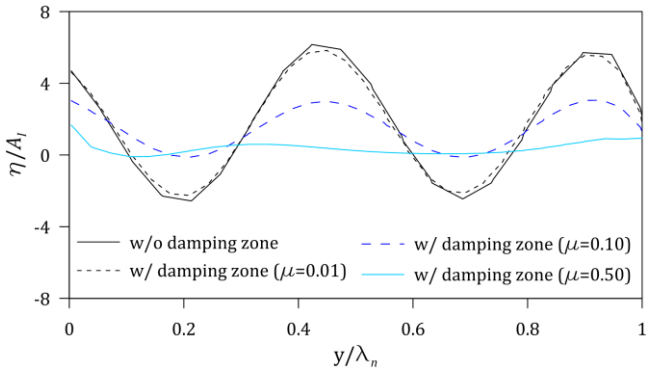

Fig. 10. Normalized free-surface elevation for the transverse direction (y) in front of the breakwater according to damping zone with various artificial coefficient (μ).

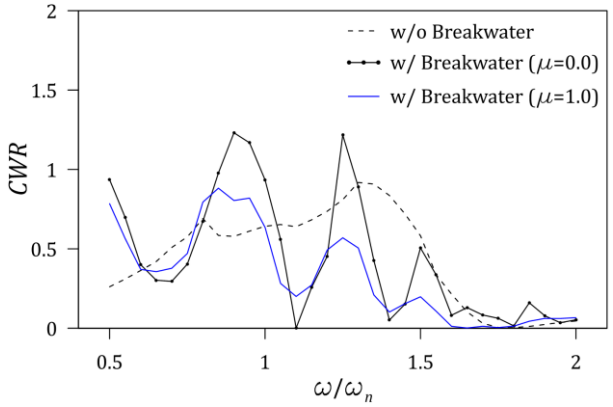

Fig. 11. Application of the damping zone to considering the wave energy dissipation due to tetrapod.

satisfying the wave energy dissipation in the breakwaters.

V. CONCLUSIONS

In this study, the breakwater effects on the performance of the oscillating water column (OWC) type wave energy converter (WEC) were analyzed by using the time-domain numerical method based on potential flow model. The turbine effect was simulated by applying the orifice model. Changes in the wave field due to breakwater can affect the performance of the OWC chamber. When the surface of the breakwater is modeled only as an impermeable wall, the effect of the breakwater on the performance of the wave field and the chamber is the largest. When the wave energy dissipation is considered based on the numerical damping zone, the performance of the OWC chamber and the wave field around the breakwater are different. Therefore, to evaluate the performance of the OWC chamber combined with breakwater more reliably, it is necessary to develop the appropriate numerical model that can consider the physical process around the breakwater. Future work will improve the numerical model to evaluate the performance of the OWC chamber by considering the wave dissipation and scattering together.

REFERENCES

[1] Falcão, António FO, and Joao CC Henriques. "Oscillating-water-column wave energy converters and air turbines: A review," *Renewable Energy* 85 (2016): 1391-1424.

[2] Torre-Enciso, Y., I. Ortubia, LI López de Aguileta, and J. Marqués. "Mutriku wave power plant: from the thinking out to the reality." *In the 8th European Wave and Tidal Energy Conference (EWTEC)*, 1:319-329, 2009.

[3] Arena, F., Romolo, A., Malara, G., Fiamma, V., and Laface, V. "The First Full Operative U-OWC Plants in the Port of Civitavecchia." *ASME 2017 36th International Conference on Ocean, Offshore and Arctic Engineering. American Society of Mechanical Engineers*, 2017.

[4] S. Park, K. H. Kim, B. W. Nam, J. S. Kim, and K. Hong, "A Study on Effects of Breakwater on Performance of OWC," *In The Thirteenth ISOPE Pacific/Asia Offshore Mechanics Symposium. International Society of Offshore and Polar Engineers*, 2018.

[5] S. Park, B. W. Nam, K. H. Kim, and K. Hong, "A Parametric Study on Oscillating Water Column Wave Energy Converter Applicable to Breakwater." *In: The 27th International Ocean and Polar Engineering Conference. International Society of Offshore and Polar Engineers,* 2017.

[6] Park, S., Kim, K. H., Nam, B. W., Kim, J. S., and Hong, K., "A Study on the Performance Evaluation of the OWC WEC Applicable to Breakwaters using CFD." *Journal of the Korean Society for Marine Environment & Energy*, 21(4), pp. 317-327, 2018.

[7] Kim, J. S., Nam, B. W., Kim, K. H., and Hong, K. Y., "Cross-sectional shape design of OWC chamber of wave energy converter applicable to breakwater." *In the 8th East Asian Workshop for Marine Environment and Energy*, 2017.

[8] Kim, K. H., Nam, B.W., Park, S. W., Kim, J. S., Kim, G. W., Lim, C. H. and Hong, K. Y., "Initial design of OWC WEC applicable to breakwater in remote island," *The 4th Asian Wave and Tidal Energy Conference (AWTEC)*, 2018.

[9] Kim, S. J., Koo, W. and Kim, M. H., "Nonliear time-domain NWT simulations for two types of a backward bent duct buoy (BBDB) compared with 2D wave-tank experiments." *Ocean Engineering* 108, 584-593, 2015

[10] Babarit, A. "A database of capture width ratio of wave energy converters." *Renewable Energy* 80: 610-628, 2015.